

# BEAM-BASED MEASUREMENT OF STRENGTH ERRORS IN QUADRUPOLE MAGNETS WITH ORBIT BUMPS

H. Koiso, H. Fukuma, Y. Funakoshi, S. Kamada, S. Matsumoto, K. Oide, and N. Yamamoto,  
KEK, Tsukuba, Japan

## Abstract

A beam-based diagnostic method with orbit bumps has been applied to measure the strength error of each quadrupole individually in the TRISTAN main ring. A pair of corrector dipoles is excited to produce a bump orbit sharply localized at a target quadrupole. By analyzing a leakage orbit outside the bump, the strength error of the target quadrupole can be estimated. Experimental results and discussions on accuracy of the measurement are reported.

## 1 INTRODUCTION

Lattice design has been getting more and more complicated in high luminosity colliders and low emittance light sources. In such machines, even small errors of machine components may significantly degrade their ultimate performance. In order to achieve high performance, beam-based diagnostics of machine errors is really important, as well as careful quality control of hardware components. If lattice errors are detected, it is necessary to find which magnets have error fields and/or misalignments. We have applied a beam-based diagnostic method with orbit bumps to measure strength errors of quadrupoles and misalignments of sextupoles in the TRISTAN main ring. We call it the "π-bump" method because orbit bump made with two corrector magnets is localized in a short section with  $\pi$  betatron phase advance. This paper focuses on the measurement of quadrupole strength errors. The measurement of misalignments will be described elsewhere in these proceedings [1].

## 2 THEORETICAL FOUNDATION OF $\pi$ BUMP METHOD

In the  $\pi$ -bump method, a pair of kicks are given at point-1 and point-2 with kick angles of  $\theta_1$  and  $\theta_2$ , respectively. The bump orbit can be locally closed by choosing the ratio of kick angles when the (1,2) element of the transfer matrix from point-1 to point-2 is zero, in other words, the betatron phase advance is  $\pi$ . A leakage orbit will arise around a ring if there exists a focusing-force error and/or a kick-angle error. As explained in the following, since these two kinds of errors contribute to a leakage orbit orthogonally, they can be determined individually from the measured leakage orbit.

The change of the equilibrium orbit  $\vec{x}_2$  outside the second bump magnet located at point-2 is given by,

$$\vec{x}_2 = \vec{\theta}_2 + T_\pi (\vec{\theta}_1 + R_{res} \vec{x}_2), \quad (1)$$

where  $R_{res}$  is the residual revolution matrix from point-2 to point-1 outside of the bump and can be written explicitly using the Twiss parameters of the ideal optics and its phase advance per turn  $\psi_0$ .  $T_\pi$  is the transfer matrix from point-1 to point-2 inside the bump and we express deviation of  $T_\pi$  using the ideal transfer matrix  $T_\pi^0$  as

$$T_\pi = T_\pi^0 + T_{error}. \quad (2)$$

$T_\pi^0$  is the ideal transfer matrix where the (1,2) element is zero and other elements can be expressed using the Twiss parameters of the ideal optics. The focusing force error is described by the second term of Eq.(2) and there are three degrees of freedom, namely  $a$ ,  $b$  and  $d$ , to satisfy the symplectic condition of  $T_\pi$ .

$$T_{error} = \begin{pmatrix} -\sqrt{\frac{\beta_{20}}{\beta_{10}}}a & \sqrt{\beta_{10}\beta_{20}}b \\ \frac{ad+a+d-(\alpha_{20}-\alpha_{10})b}{\sqrt{\beta_{10}\beta_{20}}b} & -\sqrt{\frac{\beta_{10}}{\beta_{20}}}d \end{pmatrix}, \quad (3)$$

where  $\beta_{10}$ ,  $\alpha_{10}$  and  $\beta_{20}$ ,  $\alpha_{20}$  are Twiss parameters of the ideal optics at point-1 and point-2, respectively.

Now we solve Eq.(1) for  $\vec{x}_2$  to get the leakage bump-orbit produced by a pair of kicks  $\theta_2$  at point-2 and  $\theta_1$  at point-1.

$$\vec{x}_2 = (I - T_\pi R_{res})^{-1} \left[ \begin{pmatrix} 0 \\ \theta_2 \end{pmatrix} + T_\pi \begin{pmatrix} 0 \\ \theta_1 \end{pmatrix} \right]. \quad (4)$$

The amplitude of the leakage orbit is defined by its Courant-Snyder invariant,

$$W_{cod} = \vec{X}_2^\dagger \vec{X}_2, \quad (5)$$

where  $\vec{X}_2$  is a orbit in the normal coordinate as given by

$$\vec{X}_2 = \begin{pmatrix} 1 & 0 \\ \alpha_{20} & 1 \end{pmatrix} \begin{pmatrix} \frac{1}{\sqrt{\beta_{20}}} & 0 \\ 0 & \sqrt{\beta_{20}} \end{pmatrix} \vec{x}_2. \quad (6)$$

By requiring the derivative of Eq.(5) with respect to  $\theta_2$  to be zero and by solving this differential equation for  $\theta_2$ , we get the value of  $\theta_{2min}$  that minimizes the amplitude of the leakage orbit for kick angle  $\theta_1$  at point-1.

In case of an ideal  $\pi$  section,  $\theta_{2min}$  takes a simple form Eq.(7) and there is no leakage orbit outside the bump.

$$\theta_{2min} = \sqrt{\frac{\beta_{10}}{\beta_{20}}} \theta_1. \quad (7)$$

If the optics is not the ideal one, then  $\vec{X}_2$  takes finite value even with an optimum kick of  $\theta_{2min}$ . This orbit should be considered as the leakage orbit generated by the optics error  $\vec{X}_{2b}$ . On the other hand, the leakage orbit introduced by the error kick  $\vec{X}_{2\delta}$  is given by substituting  $\theta_2 = \theta_{2min}(1 + \delta)$  into Eq.(4). Here  $\delta$  represents a relative kick error. Thus the leakage orbit is divided into two components,

$$\vec{X}_2 = \vec{X}_{2b} + \vec{X}_{2\delta}. \quad (8)$$

When  $b$  is zero,  $\vec{X}_{2b}$  becomes zero even if  $a$  and  $d$  are finite and the reverse is also true. So in view point of generation of leakage orbit,  $b$  represents the optics error and can be used to normalize  $\vec{X}_{2b}$ . In the limit of vanishing optics error,  $\vec{X}_{2b}$  normalized by  $b$  becomes,

$$\frac{\vec{X}_{2b}}{b} = \frac{\sqrt{\beta_{10}}}{2} \left\{ 1, -\cot\left(\frac{\psi_0}{2}\right) \right\} \theta_1. \quad (9)$$

When the optics is ideal, normalized  $\vec{X}_{2\delta}$  becomes,

$$\frac{\vec{X}_{2\delta}}{\delta} = \frac{\sqrt{\beta_{10}} \left\{ 1, \tan\left(\frac{\psi_0}{2}\right) \right\}}{\alpha_{10} - \alpha_{20} + 2 \tan\left(\frac{\psi_0}{2}\right)} \theta_1. \quad (10)$$

In summary, the leakage orbit is divided into two components and linearized in terms of the errors of the optics and the kick. By taking the inner product of Eqs.(9) and (10), we know that these two terms are orthogonal and can be distinguished from each other by analyzing the phase and amplitude of the leakage orbit outside the bump.

### 3 MEASUREMENTS IN THE TRISTAN MAIN RING

The lattice of the TRISTAN main ring is made up of colliding insertions, rf sections, dispersion suppressors, arcs and wiggler sections. The arcs consist of conventional FODO cells whose phase advance was set to be  $\pi/2$  during this study. The  $\pi/2$  normal cells are suitable to the  $\pi$  bump study. We can easily make  $\pi$  bumps by giving the same excitation to two correctors at the identical position in every second cell. Although the bump covers four quadrupoles, the leakage orbit is sensitive to the strength error of the quadrupole located at the peak of the bump. The sensitivity is proportional to the square of the bump height and is higher at the target quadrupole by a factor of 10. Then we can almost individually estimate the field error of the target quadrupole per bump. For the measurement of quadrupoles in straight sections, we prepared special optics to adjust the phase difference between steerings to  $\pi$ . In this case, the kick angles were chosen as Eq.(7).

Out of 400 quadrupoles in the ring, 220 were measured; 76 QF's and 80 QD's in the arcs and 64 in the straight sections. Quadrupoles in the dispersion suppressors and in the wiggler sections remain unmeasured since it is difficult to arrange the optics to easily create  $\pi$  bumps. When we formed bumps at the quadrupoles in the arcs, we turned off the sextupoles so that we can eliminate their effects. Although the stored beam current was limited to less than 100  $\mu$ A because of no chromaticity correction, our position monitors have sufficient sensitivity.

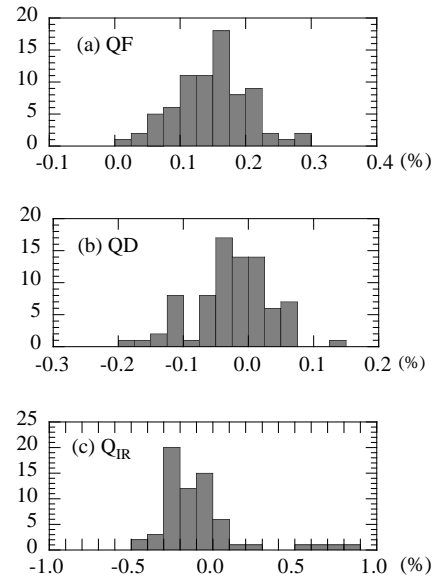


Figure 1: Relative-strength errors of quadrupoles; a) QF's, b) QD's, and c) quadrupoles in the straight sections.

The closed orbit around the ring is measured by 392 position monitors attached to quadrupoles. We measured three sequential orbit data for one bump; 1) bump off (*OrbitA*), 2) bump on (*OrbitB*), and 3) bump off (*OrbitC*), to check the orbit drift during measurements. When we observed significant difference between Orbit A and C, we rejected the data. The leakage orbit to be analyzed was obtained by *OrbitB-OrbitC* or *OrbitB-OrbitA*. The measurements of horizontal-focusing(-defocusing) quadrupoles were done by horizontal (vertical) bumps. The bump height applied was typically 10mm.

In data analysis, the leakage orbit was corrected by two kinds of correctors; the virtual thin steering at the edge of the target quadrupole and one of the two steerings employed to make a bump. All calculations concerning the data analysis were done by the code SAD developed at KEK [2]. From the kick angles of these correctors,  $\theta_{quad}$  and  $\theta_{st}$ , we can estimate the strength error of the target quadrupole and the imbalance of the two steerings.  $\theta_{quad}$  is related to the strength error  $\Delta K$  by  $\theta_{quad} = \int \Delta K(s)x(s)ds$  where  $x$  is the bump height. In this study,  $\theta_{quad}$  was of the order of several  $\mu$ rad.

Figure 1 shows the distributions of the relative strength errors of the quadrupoles. The QF's (QD's) are fed by a single power supply. The standard deviations of the strength er-

rors of QF's and QD's are  $5.7 \times 10^{-4}$  and  $5.9 \times 10^{-4}$ , respectively, which are consistent with the observation from the field measurement done before the installation [3]. Large errors were observed in final quadrupoles in the colliding insertions. This is because we measured these quadrupoles at much lower excitation than during usual operation. At the usual excitation, the errors of these quadrupoles became similar to the others in the straight sections.

## 4 PRECISION OF THE MEASUREMENT

In most cases, we applied only one bump for one quadrupole because of the limited machine time. However, a more reliable way is to do the  $\pi$ -bump measurement several times for each quadrupole by changing the bump height, because it allows to correctly estimate the strength errors of the quadrupole, even with some nonlinearities in the lattice. This was done for a few quadrupoles of different types.

In the case of QF's, this kind of measurements is proved to be essential because the kick is not linearly dependent on the bump height as shown in Fig. 2. One possible source of the nonlinearity is the remnant field of a sextupole placed near the target quadrupole. We estimated the integrated sextupole field to be  $k_{2,S} F_{rem} = 0.039$  by a polynomial fitting, which is not far from the result of the field measurement ( $k_{2,S} F_{rem} = 0.029$  and  $k_{2,S} D_{rem} = 0.039$ ). We can extract the quadrupole strength error by taking a linear component in the fitting. Figure 1a) shows the data after subtraction of the sextupole effect assuming  $k_{2,S} F_{rem} = 0.029$ .

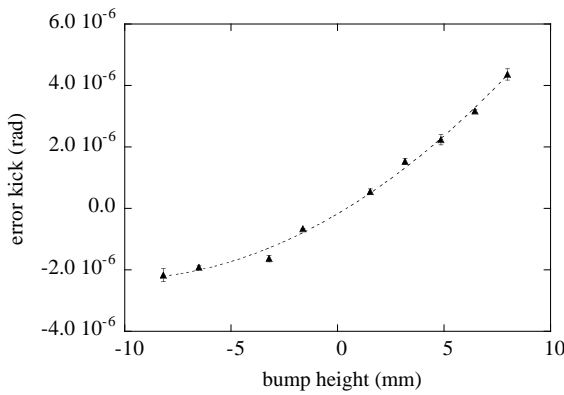


Figure 2: The error kick by a QF vs. the horizontal bump height.

In the case of QD's, the data is sufficiently linear in the bump height as shown in Fig. 3. The vertical bump orbit at a sextupole produces a kick proportional to the bump height  $y$  as  $\Delta y'_{SD} = k_{2,SD} D_{rem} x_{mis} y$ , where  $x_{mis}$  is the horizontal misalignment of the sextupole. This effect can not be separated from a kick by the strength error of the quadrupole because of its linearity. If  $x_{mis} = 1\text{mm}$  and  $y = 10\text{mm}$ ,  $\Delta y'_{SD}$  amounts to  $0.4\mu\text{rad}$ , which introduces 20% uncertainty in the estimation of a quadrupole kick.

In order to estimate practically the statistical accuracy of our measurement, we analyzed the leakage orbit without

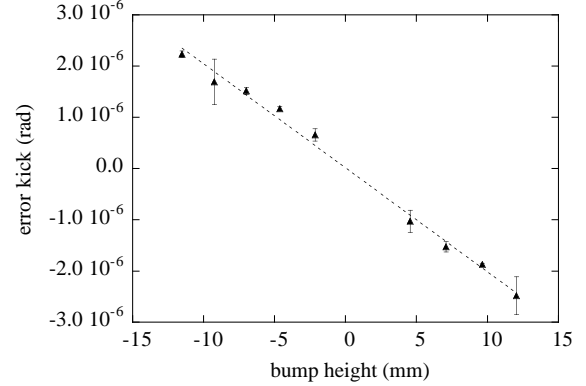


Figure 3: The error kick by a QD vs. the vertical bump height.

bumps by the same procedure as with bumps and obtained the fake kick due to the quadrupole strength error. By 55 samples, we estimated the accuracy to be  $0.2\mu\text{rad}$ , which is sufficiently small compared to typical kicks by quadrupoles. In Figs. 2 and 3, the error bars show the difference between two redundant data of *OrbitB-OrbitA* and *OrbitB-OrbitC*. In most cases in the figures, the error bars are consistent with  $0.2\mu\text{rad}$ . Data points with larger error bars are considered to be affected by the orbit drift. The fitting results in Figs. 2 and 3 are  $\Delta k/k = (2.250 \pm 0.063) \times 10^{-3}$  and  $\Delta k/k = (1.118 \pm 0.036) \times 10^{-3}$ , respectively.

## 5 CONCLUSIONS

The strength errors of quadrupoles were successfully measured by the  $\pi$ -bump method in the TRISTAN Main Ring. The relative strength errors of the order of  $10^{-4}$  were detected with statistical accuracy of the order of  $10^{-5}$  by eliminating bad data affected by orbit drifts.

## 6 ACKNOWLEDGMENTS

We thank Dynamic Aperture Issues Working Group and TRISTAN Operation Group for supporting our study.

## 7 REFERENCES

- [1] N. Yamamoto et al., in these proceedings.
- [2] <http://130.87.74.156/SAD/sad.html>.
- [3] N. Kumagai, K. Egawa, K. Takayama, and M. Kihara, IEEE Trans. Magnet vol.24, 1319 (1988).